

Letter

First Assessment of Geophysical Sensitivities from Spaceborne Galileo and BeiDou GNSS-Reflectometry Data Collected by the UK TechDemoSat-1 Mission

Matthew L. Hammond ^{1,*} , Giuseppe Foti ¹ , Jonathan Rawlinson ² ,
Christine Gommenginger ¹, Meric Srokosz ¹ , Lucinda King ^{2,3}, Martin Unwin ² and
Josep Roselló ⁴

¹ National Oceanography Centre, Southampton SO14 3ZH, UK; g.foti@noc.ac.uk (G.F.); cg1@noc.ac.uk (C.G.); mas@noc.ac.uk (M.S.)

² Surrey Satellite Technology Ltd., Guildford GU2 7YE, UK; J.Rawlinson@sstl.co.uk (J.R.); l.s.king@surrey.ac.uk (L.K.); M.Unwin@sstl.co.uk (M.U.)

³ Surrey Space Centre, University of Surrey, Guildford GU2 7XH, UK

⁴ European Space Agency, ESTEC, 2201 AZ Noordwijk, The Netherlands; Josep.Rosello@esa.int

* Correspondence: matthew.hammond@noc.ac.uk

Received: 14 August 2020; Accepted: 8 September 2020; Published: 10 September 2020



Abstract: The UK's TechDemoSat-1 (TDS-1), launched 2014, has demonstrated the use of global positioning system (GPS) signals for monitoring ocean winds and sea ice. Here it is shown, for the first time, that Galileo and BeiDou signals detected by TDS-1 show similar promise. TDS-1 made seven raw data collections, recovering returns from Galileo and BeiDou, between November 2015 and March 2019. The retrieved open ocean delay Doppler maps (DDMs) are similar to those from GPS. Over sea ice, the Galileo DDMs show a distinctive triple peak. Analysis, adapted from that for GPS DDMs, gives Galileo's signal-to-noise ratio (SNR), which is found to be inversely sensitive to wind speed, as for GPS. A Galileo track transiting from open ocean to sea ice shows a strong instantaneous SNR response. These results demonstrate the potential of future spaceborne constellations of GNSS-R (global navigation satellite system–reflectometry) instruments for exploiting signals from multiple systems: GPS, Galileo, and BeiDou.

Keywords: global navigation satellite system; GNSS reflectometry; GNSS-R; TechDemoSat-1; TDS-1; ocean wind speed; sea ice; Galileo; BeiDou

1. Introduction

Global navigation satellite system–reflectometry (GNSS-R) is a rapidly developing approach to Earth observation that makes use of signals of opportunity from global navigation satellite systems (GNSS), which have been reflected from the Earth's surface. GNSS-R using global positioning system (GPS) signals has already proven capable of accurate retrieval of ocean surface roughness and wind speed [1–4] as well as of sea-ice presence [5–7]. The technology is particularly promising as it does not require a dedicated transmitter, thereby reducing cost, mass, and power requirements of the receivers. Past and present spaceborne GNSS-R missions (UK Disaster Monitoring Constellation (UK-DMC) [8], TechDemoSat-1 (TDS-1) [9], CYclone Global Navigation Satellite System (CYGNSS) [10], BuFeng-1 [11]) have been focused on collecting reflected GPS signals. In principle, however, the existing receivers can be adapted to the acquisition of navigation signals within a similar frequency spectrum transmitted by other navigation systems (including the European Galileo and the Chinese BeiDou), which potentially allows for a significantly larger number of simultaneous reflections available within the footprint of the GNSS-R sensor, which should translate into higher sampling. The combination of a large number of

simultaneous reflections alongside the potential for affordable multi-satellite constellations [12] offers the opportunity to build up an Earth observation system delivering global coverage and high revisit frequency on a relatively low budget. However, enabling GNSS-R sensors to use signals incoming from multiple navigation systems requires extensive adaptation work including signal processing optimization to account for different signal characteristics.

Geophysical inversion using GNSS signals from constellations other than GPS has already been achieved in the past, including ground experiments exploiting GLObal NAvigation Satellite System (GLONASS) and Galileo [13,14] and airborne experiments using BeiDou, GPS, GLONASS, and Galileo [15–17]. A limited number of spaceborne collections of reflected signals transmitted by the Galileo In-Orbit Validation Experiment (GIOVE) were collected by the UK-DMC mission, although hardware limitations led to significant signal attenuation [18]. Multi-constellation sea surface altimetry using both Galileo and GPS has been conducted using raw data from the CYGNSS mission [19].

During the lifetime of the TDS-1 mission (2014–2019), the receiver aboard TDS-1 was periodically operated in raw acquisition mode (i.e., bypassing on-board signal processing) and raw sampled data were collected and relayed to the ground to be processed later. Some of these collections were timed to include non-GPS reflected signals such as Galileo signals. In this study we present data from seven Galileo-reflected tracks, as well as one BeiDou-3 track. To the author's knowledge, this possibly represents the largest satellite Galileo reflectometry record at the time of writing. An initial analysis of available signal-to-noise ratio (SNR) is presented here, together with a preliminary assessment of the sensitivity of Galileo reflections to surface characteristics.

2. Materials and Methods

Seven Galileo-reflected tracks were acquired between November 2015 and March 2019, originating from six different transmitters, as well as one BeiDou-3 track collected in March 2019. Each track was of 130 s length, except the BeiDou-3 track which was 65 s long. All data were acquired by TDS-1 in raw mode and later processed on the ground by Surrey Satellite Technology Ltd. (SSTL) (Guildford, UK) [20]. Two parallel tracks, each 130 s long and ~200 km apart, were acquired simultaneously on 18 October 2018, the first being transmitted by GPS PRN26, and the second by Galileo E31, allowing an initial assessment of neighbouring Galileo and GPS reflections collected by the same instrument. The bandwidth of TDS-1 front-end was set to 2.5 Mhz for all collections in this work, except for the final set (targeting E26) where the bandwidth was set to 4.2 MHz. All samples were processed on the ground using different coherent integration times. Assuming that coherent integration interval is suitably selected to avoid self-destructive signal interference, coherent delay Doppler maps (DDMs) based on longer integrations are expected to provide a higher SNR [21]. The 1 ms coherent integration used by the on-board TDS-1 correlator to process reflected GPS signals is relatively short compared to the Galileo code length of 4 ms (the GPS L1 C/A signal has a code length of 1 ms) and refinement of the signal processing strategy, possibly by including longer integration times, may be required to achieve optimal retrieval performance from reflected Galileo data.

The GPS DDMs were processed using coherent integration times of 1 ms, corresponding to the coherent integration time used by the TDS-1 on-board GNSS-R processor; and 2 ms, which should provide a higher SNR. Galileo returns were processed using two different coherent integration times: 1 ms (i.e., the same as for GPS), and 4 ms (the same as the Galileo code length). BeiDou-3 data were processed similarly, using 1 ms and 4 ms coherent integration times. In all cases, incoherent accumulation time was adapted to obtain DDMs consistently output at 1 Hz. The longer of the two coherent integration times for each system is analysed here as they should provide a stronger SNR, making key features easier to recognise, (side-by-side comparisons of DDMs obtained using different coherent integration times can be found in the supporting information, Figures S1 and S2, alongside their processing settings in Table S1).

Due to the unavailability of corresponding metadata necessary for radiometric calibration of these experimental collections, the preliminary analysis presented here is limited to SNR as a primary observable. The SNR is estimated from individual DDMs of BeiDou-3, Galileo, and GPS reflected data, and the observable is defined as the ratio of the DDM power in the signal and the noise boxes using the DDM characterization and peak power location mechanism described by [4]. The noise power box (N) is fixed in DDM space and of constant size, covering all Doppler frequency bins and the first four delay (1 chip) bins in the signal free area of the DDM. The signal box (S) also has a constant size of four delay bins (1 chip) and a size of ~ 3000 Hz in Doppler, dependent on the Doppler resolution of a given processing setting.

To assess the sensitivity of SNR to surface parameters, model reanalysis wind-speed and observational sea-ice concentration fields were used. Wind speed fields were obtained from the European Centre for Medium-Range Weather Forecasts (ECMWF) ERA-5 High Resolution (HRES) reanalysis model which is available with a spatial resolution of 31 km and a temporal resolution of 1 h and is shown to provide favourable performance relative to scatterometers [22]. Sea-ice concentration fields were obtained from the European organisation for the Exploitation of METeorological SATellites (EUMETSAT) Ocean and Sea-ice Satellite Application Facilities (OSISAF) Special Sensor Microwave Imager/Sounder (SSMIS) sea-ice concentration maps, which are made available on a daily 10 km polar stereographic grid.

3. Results

3.1. Ocean Wind Speed

Figure 1 shows example DDMs taken over the open ocean from signals originating from GPS, Galileo, and BeiDou-3. The Galileo and GPS DDMs were collected simultaneously on 18 October 2018. It is clear that all three DDMs show the same general shape. However there are some differences in SNR levels that will originate from differences in signal geometry, surface conditions, and the transmitted signals. It is notable that the GPS DDM delivers the highest SNR (~ 1.5 dB greater than BeiDou-3 and Galileo), despite this surface having the highest wind speed conditions.

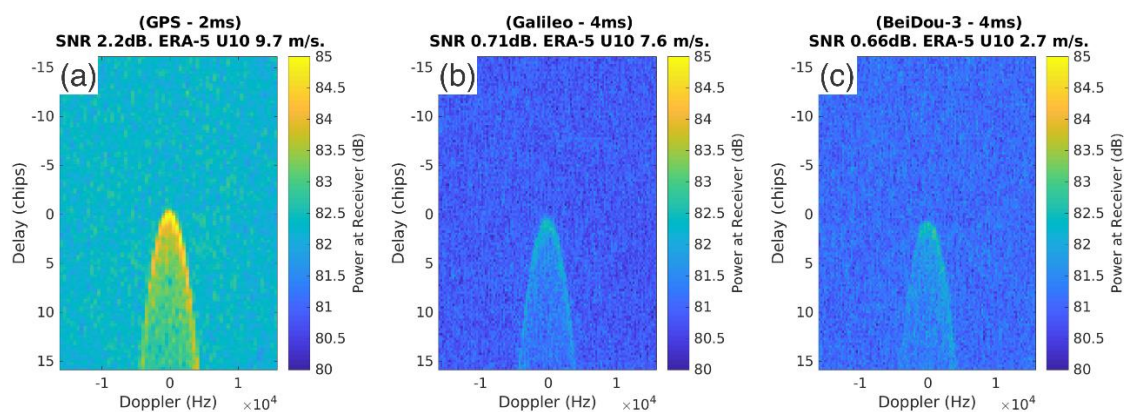


Figure 1. Delay Doppler maps (DDMs) retrieved over the open ocean from (a) global positioning system (GPS) (b) Galileo, and (c) BeiDou-3. All DDMs show a similar shape with a typical DDM “horseshoe”, albeit with different SNR responses, dependent on different surface conditions, bistatic geometry, and signal characteristics. Note that these DDMs were collected over the open ocean with different surface parameters, including wind speed. GPS and Galileo DDMs were collected simultaneously on parallel tracks on 18 October 2018 but the specular points had an average spatial separation of ~ 214 km.

An example Galileo track is shown in Figure 2 collected on 11 November 2015, over the ocean near the East Coast of North America. Figure 2a shows the location of the track within the ERA-5 wind speed field at the nearest hour, whilst Figure 2b shows the SNR of the track relative to the ERA-5 wind speed at the nearest point in space and time. Results indicate a well-defined inverse relationship between Galileo SNR and wind speed, similar to what has been found in previous work based on reflected GPS observations. It is also noticeable that sensitivity is reduced at higher wind speeds, where signal power is lower and the effect of noise variance becomes more visible. This Galileo track is of particularly low SNR which translates to increased dispersion of the observable already at moderate wind speeds. This track shows for the first time a clear geophysical sensitivity of spaceborne Galileo returns to ocean wind speed conditions.

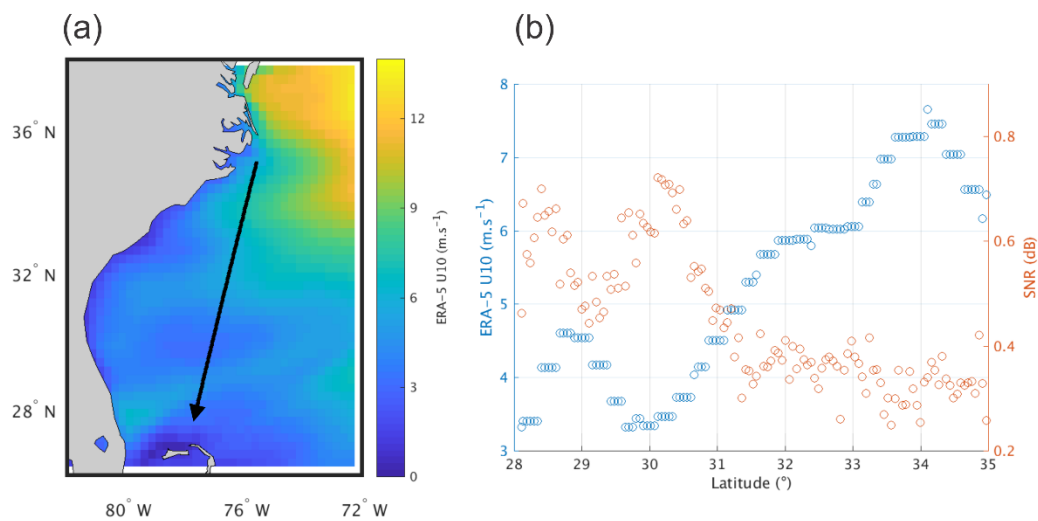


Figure 2. (a) Shows the location of one Galileo track on 11 November 2015 (descending pass), transmitted by E19, overlaid on the ERA-5 wind speed field, (b) shows that Galileo SNR and wind speed present a clear along-track inverse relationship. ERA-5 U10 indicates the wind speed at 10 m above the ocean surface.

Figure 3 shows results based on all TDS-1 Galileo raw collections available at present (2015–2019), clearly showing that SNR generally tends to decrease as surface wind speed increases. The line of best fit follows a simple exponential similar to the geophysical model function (GMF) derived from GPS reflected data, and adopted in the National Oceanography Centre (NOC) calibrated bistatic radar equation (C-BRE) ocean wind speed algorithm [4]. Specifically, the line of best fit follows:

$$\text{SNR} = A e^{B \cdot U10} + C \quad (1)$$

where $A = 1.2$, $B = -0.5$, $C = 0.3$, and $U10$ is the wind speed at a height of 10 m above ocean surface.

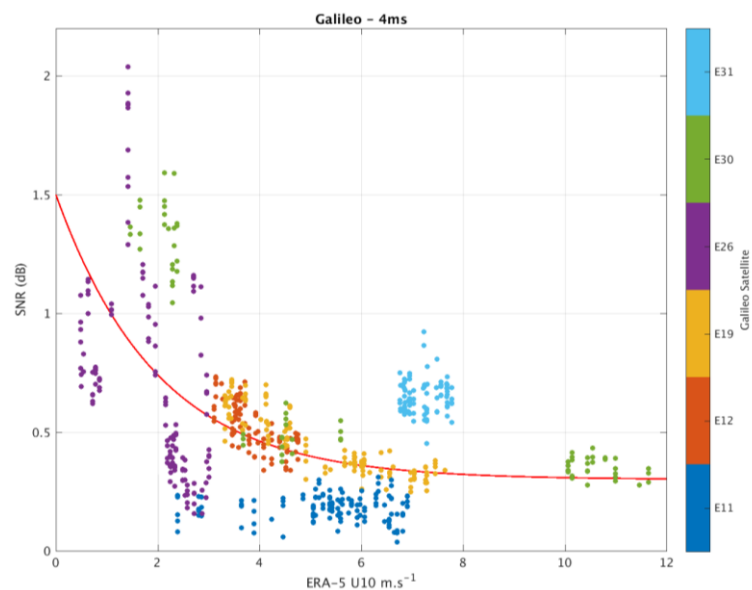


Figure 3. Relationship between Galileo signal-to-noise ratio (SNR) and ERA-5 wind speed, coloured by transmitting Galileo satellite and associated Pseudorandom Noise code (PRN) (Exx). The red line shows the line of best fit using an exponential curve, similar in shape to the geophysical model function (GMF) that was found for GPS reflected signals. These preliminary results show some promise for the future development of an ocean wind speed retrieval algorithm based on reflected Galileo signals. See Supporting Figure S3 for a similar plot coloured by antenna gain towards the specular point (AGSP).

3.2. Sea Ice

Figure 4 shows GPS and Galileo DDMs collected on 18 October 2018 over sea-ice (no BeiDou-3 reflected data are currently available over sea-ice). DDMs over sea-ice show similar “k-shapes” as described by [6], i.e., showing both a horseshoe and Doppler side-lobes. The Doppler side-lobes, although faint, are clearly much sharper and better defined in the case of the Galileo DDM. Of the two DDMs, a higher SNR is seen in the GPS collection; the peak in the Galileo DDM is noticeably sharper than the GPS DDM meaning that the currently selected size of the signal box is likely too large, thus picking up information from pixels too far away from the peak, and leading to non-optimal estimation of the reflected SNR.

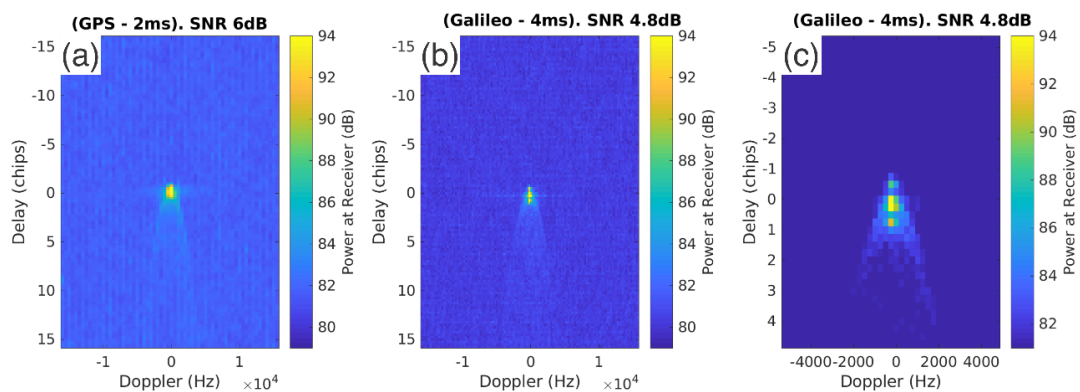


Figure 4. DDMs retrieved on 18 October 2018 over sea-ice from GPS (a) and Galileo (b), and a close up of the peak area of the Galileo DDM (c). The GPS and Galileo DDMs were collected from parallel tracks having an average spatial separation of ~ 214 km. Both DDMs show a similar, albeit faint, “k-shape” form over sea-ice—showing some promise for the development of sea-ice detection algorithms for either navigation system, although these will require adaptation for a number of factors including different average SNR and distinctive shape of the correlated Galileo waveform (triple peak).

In Figure 4c a close-up is shown of the Galileo DDM signal; this shows a distinctive triple peak in delay space. This triple peak derives from the modulation strategy (composite binary offset carrier (CBOC)) used by Galileo E1OS signals, whereas binary phase shift keying (BPSK) is adopted in GPS L1 C/A. Note that because of the input filtering associated with the TDS-1 RF chain only the BOC(1, 1) component is collected by the instrument. The SNRs of each specular point of the two simultaneous GPS and Galileo tracks collected in October 2018 are shown in Figure 5. There is a marked increase in SNR (~ 2 dB for Galileo, ~ 4 dB for GPS) as the specular point transitions from the open ocean on to the sea-ice edge. This shows that Galileo signals are responding to changes in the nature of the geophysical surface in a similar way to GPS.

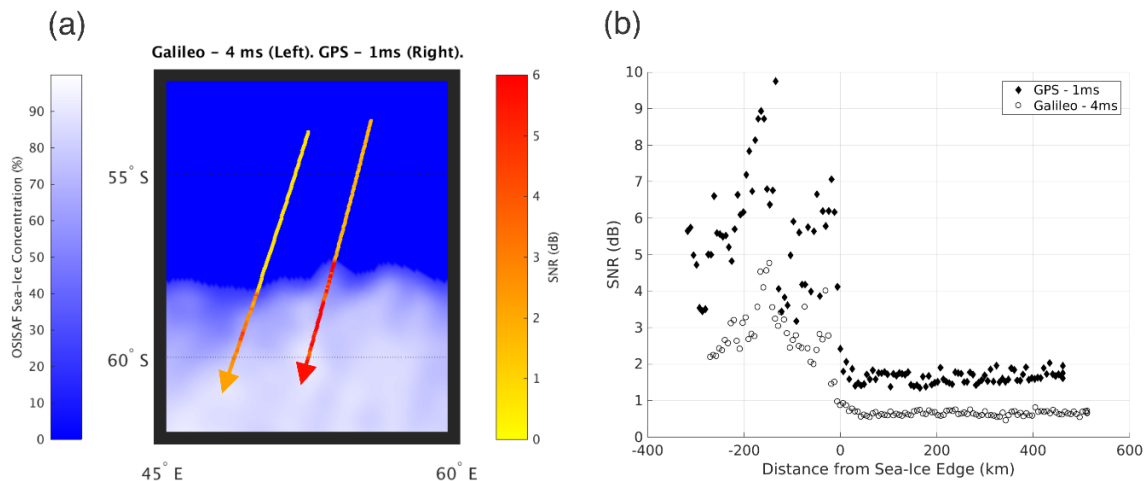


Figure 5. (a) TechDemoSat-1 (TDS-1) tracks retrieved on 18 October 2018 (descending pass) including transition from open ocean to sea-ice from GPS (right) and Galileo (left) reflected signals. (b) Received SNR for the two tracks against distance from sea-ice edge. Along-track SNR shows a strong response as the specular point location transitions on to sea-ice, indicating high sensitivity of both Galileo and GPS to surface characteristics.

4. Discussion

4.1. Ocean Wind Speed

In Figure 1, it is notable that in the current processing configuration the GPS DDM delivers the highest SNR (~ 1.5 dB greater than BeiDou-3 and Galileo), despite this surface having the highest wind speed conditions. This may result from differences in the signal processing including available signal bandwidth, front-end filtering effects, and coherent integration times. Transmitted GPS L1 C/A signals have a bandwidth of ~ 2 MHz, whilst Galileo E1OS and BeiDou-3 B1C services have a wider spectrum of ~ 4 MHz (if only the BOC(1, 1) component is taken into account), a change necessitated in part by the different modulation type used. Figures S4 and S5 show the Galileo signal power spectral density and TDS-1 frequency response. In the context of remote-sensing applications, wider bandwidth of reflected signals (as filtered by the receiver front-end) are expected to be associated with increased horizontal surface resolution, but such reduced scattering area will also result in reduced reflected power, thereby lowering the available SNR [18]. Lower available signal-to-noise ratios have the potential to reduce the accuracy of scatterometric estimates of surface parameters; however, this effect could be at least partially mitigated by the use of longer integration times, also courtesy of the smaller Galileo footprint which potentially allows for longer integration at a given bandwidth. Further work to optimize signal processing of Galileo and BeiDou-3 returns for remote sensing applications by carefully balancing the above factors will likely help mitigate some of the current limitations.

At first glance, the shape of the SNR response to wind-speed (Figure 3) seems to apply to all Galileo transmitters examined over ~ 4 years of collections. However, there are some notable exceptions to this;

for example, E11 appears to show no apparent response to wind speed, this is likely associated with contamination from noise variance as the average SNR level of this E11 subset appears to be particularly low (average of ~ 0.18 dB). E11 is an in orbit validation (IOV) satellite with a lower transmit power (95 W) than the Full Operational Capability (FOC) satellites (254–273 W) [23]. Conversely, the subset including reflected data from Galileo E31 appears to achieve a higher-than-average SNR (average of ~ 0.65 dB). This likely results from the relatively high antenna gain towards the specular point (AGSP) of the E31 collections (Figure S3—supporting information). In summary, as the observables considered so far are not radiometrically calibrated, some of these effects are most likely related to factors including different equivalent isotropic radiation power (EIRP) between Galileo satellites, viewing geometry, location of the specular point in the field of view of the instrument, and associated antenna gain.

4.2. Sea Ice

The distinctive triple peak of the correlation waveform (Figure 4c) is usually invisible over the open ocean, especially at moderate to high wind speeds, primarily because of the relatively weak coherent component typically incoming from rough ocean surfaces, and also because of the weighted sum (convolution) of the many individual impulse responses (Woodward ambiguity function) from the different individual “facets” where the scattering is taking place, which are closer than the width of the Woodward ambiguity function itself. Again, further work is required to optimize the Galileo SNR estimation over strongly coherent surfaces, also by taking into account the distinctive shape of the Galileo auto-correlation function.

The increased SNR over sea ice (Figure 5) derives from the fact that the scattering regime at the surface mainly consists of a dominant coherent component with energy primarily incoming from a substantially smaller glistening zone centred on the specular point. The second observation is that, as observed above, GPS returns routinely achieve higher SNR than Galileo, at least with the current processing setup. This may in part be due to the non-optimal front-end bandwidth set-up adopted during the acquisition of these initial Galileo collections (2.5 MHz rather than 4.2 MHz). It is also clear that the SNR shows a substantial range over the sea-ice surface (~ 3 dB in the case of Galileo), which may support the development of further ice characterisation algorithms, beyond simple detection of sea-ice presence. This would likely require more information from the DDM [24], but it would be interesting to determine with more data how the signals from Galileo compare to GPS in retrieving this information, particularly in regard to the wider Galileo bandwidth and different correlated waveform which might provide different sensitivity to ice properties.

5. Conclusions

A first comparison between forward-scattered correlated power maps incoming from Galileo, BeiDou and GPS constellations is presented in this study, using ground-processed data collected between November 2015 and March 2019 by the UK TDS-1 mission. For similar surface conditions, results show that Galileo reflected signals generally achieve lower SNR than those from GPS, at least when using the current signal processing design and setup. According to theory, the wider bandwidth of Galileo reflections may correspond to improved surface resolution, but further work is needed for experimental verification. It is clear from this study that signal processing optimization is of critical importance for the design and development of future GNSS-R missions targeting the exploitation of multiple navigation systems. Demonstrated here for the first time is sensitivity of Galileo reflectance to geophysical parameters as detected by a spaceborne receiver, with both ocean wind speed and sea-ice presence shown to have similar relationships to reflected GPS signals, at least in shape. Unfortunately, due to the limited volume of available reflected BeiDou data at present, no conclusive analysis of the geophysical sensitivity of BeiDou signals can be carried out. A greater volume of data from a variety of surface conditions is required for detailed characterisation of the sensitivity of SNR to other sea surface conditions from both Galileo and BeiDou. This work demonstrates the promising nature of

spaceborne GNSS-R systems for future wind speed retrieval and sea-ice detection using signals from a combination of different navigation systems, including GPS, Galileo, and BeiDou.

Supplementary Materials: The following are available online at <http://www.mdpi.com/2072-4292/12/18/2927/s1>, Figure S1: Galileo and GPS DDM Processing Examples, Figure S2: BeiDou DDM Processing Examples, Figure S3: Galileo SNR Wind Speed Relationship by AGSP, Figure S4: Power spectral density of the Galileo E1OS signal, Figure S5: Frequency response of the TDS-1 front-end, Table S1: List of DDM processor settings.

Author Contributions: Methodology and investigations: M.L.H.; Software: M.L.H., G.F., J.R. (Jonathan Rawlinson); Data Curation: J.R. (Jonathan Rawlinson), L.K.; writing—original draft preparation: M.L.H.; writing—review and editing: All; supervision: G.F., C.G., M.S., M.U.; project administration: J.R. (Josep Roselló). All authors have read and agreed to the published version of the manuscript.

Funding: This work was funded by ESA contract 4000123436/NL/FF/gp. G.F. was supported by NERC grant no. NE/N018095/1 (Ocean Regulation of Climate by Heat and Carbon Sequestration and Transports, ORCHESTRA).

Acknowledgments: ERA-5 data were generated using Copernicus Climate Change Service Information [2019] neither the European Commission nor ECMWF is responsible for any use that may be made of the Copernicus Information or Data it contains. OSISAF data were made available by EUMETSAT, copyright © 2020 EUMETSAT.

Conflicts of Interest: The authors declare no conflict of interest.

References

1. Komjathy, A.; Armatys, M.; Masters, D.; Axelrad, P.; Zavorotny, V.; Katzberg, S. Retrieval of ocean surface wind speed and wind direction using reflected GPS signals. *J. Atmos. Ocean. Technol.* **2004**, *21*, 515–526. [[CrossRef](#)]
2. Katzberg, S.J.; Torres, O.; Ganoe, G. Calibration of reflected GPS for tropical storm wind speed retrievals. *Geophys. Res. Lett.* **2006**, *33*, 1–5. [[CrossRef](#)]
3. Gleason, S.; Gebre-Egziabher, D. *GNSS Applications and Methods*; Artech House: Boston, MA, USA, 2009.
4. Foti, G.; Gommenginger, C.; Jales, P.; Unwin, M.; Shaw, A.; Robertson, C.; Rosello, J. Spaceborne GNSS reflectometry for ocean winds: First results from the UK TechDemoSat-1 mission. *Geophys. Res. Lett.* **2015**, *42*, 5435–5441. [[CrossRef](#)]
5. Yan, Q.; Huang, W. Spaceborne GNSS-R Sea Ice Detection Using Delay-Doppler Maps: First Results from the U.K. TechDemoSat-1 Mission. *IEEE J. Sel. Top. Appl. Earth Obs. Remote Sens.* **2016**, *9*, 4795–4801. [[CrossRef](#)]
6. Alonso-Arroyo, A.; Zavorotny, V.U.; Camps, A. Sea Ice Detection Using U.K. TDS-1 GNSS-R Data. *IEEE Trans. Geosci. Remote Sens.* **2017**, *55*, 4989–5001. [[CrossRef](#)]
7. Cartwright, J.; Banks, C.J.; Srokosz, M. Sea Ice Detection Using GNSS-R Data from TechDemoSat-1. *J. Geophys. Res. Ocean.* **2019**, *124*, 5801–5810. [[CrossRef](#)]
8. Unwin, M.; Gleason, S.; Brennan, M. The Space GPS Reflectometry Experiment on the UK Disaster Monitoring Constellation Satellite. In Proceedings of the 16th International Technical Meeting of the Satellite Division of The Institute of Navigation (ION GPS/GNSS 2003), Portland, OR, USA, 9–12 September 2003; pp. 2656–2663.
9. Unwin, M.; Jales, P.; Tye, J.; Gommenginger, C.; Foti, G.; Rosello, J. Spaceborne GNSS-Reflectometry on TechDemoSat-1: Early Mission Operations and Exploitation. *IEEE J. Sel. Top. Appl. Earth Obs. Remote Sens.* **2016**, *9*, 4525–4539. [[CrossRef](#)]
10. Ruf, C.; Unwin, M.; Dickinson, J.; Rose, R.; Rose, D.; Vincent, M.; Lyons, A. CYGNSS: Enabling the Future of Hurricane Prediction. *IEEE Geosci. Remote Sens. Mag.* **2013**, *1*, 52–67. [[CrossRef](#)]
11. Niu, X.; Lu, F.; Liu, Y.; Jing, C.; Wan, B. *Application and Technology of Bufeng-1 GNSS-R Demonstration Satellites on Sea Surface Wind Speed Detection*; Springer: Singapore, 2020; Volume 650, ISBN 9789811537066.
12. Carreno-Luengo, H.; Camps, A.; Via, P.; Munoz, J.F.; Cortiella, A.; Vidal, D.; Jane, J.; Catarino, N.; Hagenfeldt, M.; Palomo, P.; et al. 3Cat-2-An Experimental Nanosatellite for GNSS-R Earth Observation: Mission Concept and Analysis. *IEEE J. Sel. Top. Appl. Earth Obs. Remote Sens.* **2016**, *9*, 4540–4551. [[CrossRef](#)]
13. Qian, X.; Jin, S. Estimation of Snow Depth from GLONASS SNR and Phase-Based Multipath Reflectometry. *IEEE J. Sel. Top. Appl. Earth Obs. Remote Sens.* **2016**, *9*, 4817–4823. [[CrossRef](#)]
14. Ma, H.; Antoniou, M.; Pastina, D.; Santi, F.; Pieralice, F.; Bucciarelli, M.; Cherniakov, M. Maritime Moving Target Indication Using Passive GNSS-Based Bistatic Radar. *IEEE Trans. Aerosp. Electron. Syst.* **2018**, *54*, 115–130. [[CrossRef](#)]

15. Carreno-luengo, H.; Amèzaga, A.; Vidal, D.; Olivé, R.; Munoz, J.F. First Polarimetric GNSS-R Measurements from a Stratospheric Flight over Boreal Forest. *Remote Sens.* **2015**, *7*, 13120–13138. [[CrossRef](#)]
16. Fabra, F.; Cardellach, E.; Ribó, S.; Li, W.; Rius, A.; Arco-Fernández, J.C.; Nogués-Correig, O.; Praks, J.; Rouhe, E.; Seppänen, J.; et al. Is accurate synoptic altimetry achievable by means of interferometric GNSS-R? *Remote Sens.* **2019**, *11*, 505. [[CrossRef](#)]
17. Wang, X.; Sun, Y.; Du, Q.; Wang, D.; Wu, D.; Cai, Y.; Wu, C.; Bai, W.; Xia, J.; Li, W. An integrated GNSS remote sensing instrument and its first GNSS-R airborne experiment. In Proceedings of the International Geoscience Remote Sensing Symposium 2016, Beijing, China, 10–15 July 2016; pp. 4827–4830. [[CrossRef](#)]
18. Jales, P. *Spaceborne Receiver Design for Scatterometric GNSS Reflectometry*; University of Surrey: Guildford, UK, 2012.
19. Cardellach, E.; Li, W.; Rius, A.; Semmling, M.; Wickert, J.; Zus, F.; Ruf, C.S.; Buontempo, C. First Precise Spaceborne Sea Surface Altimetry with GNSS Reflected Signals. *IEEE J. Sel. Top. Appl. Earth Obs. Remote Sens.* **2020**, *13*, 102–112. [[CrossRef](#)]
20. Surrey Satellite Technology Ltd. *MERRByS Product Manual v7*. 2019, 28–30. 2019. Available online: http://merrbys.co.uk/wp-content/uploads/2019/12/0248366_MERRByS-Product-Manual-GNSS-Reflectometry-on-TDS-1-with-the-SGR-ReSI_007.pdf (accessed on 5 September 2020).
21. Hajj, G.A.; Zuffada, C. Theoretical description of a bistatic system for ocean altimetry using the GPS signal. *Radio Sci.* **2003**, *38*. [[CrossRef](#)]
22. Belmonte Rivas, M.; Stoffelen, A. Characterizing ERA-interim and ERA5 surface wind biases using ASCAT. *Ocean Sci. Discuss.* **2019**, *15*, 1–31. [[CrossRef](#)]
23. Steigenberger, P.; Thielert, S.; Montenbruck, O. GNSS satellite transmit power and its impact on orbit determination. *J. Geod.* **2018**, *92*, 609–624. [[CrossRef](#)]
24. Rodriguez-Alvarez, N.; Holt, B.; Jaruwatanadilok, S.; Podest, E.; Cavanaugh, K.C. An Arctic sea ice multi-step classification based on GNSS-R data from the TDS-1 mission. *Remote Sens. Environ.* **2019**, *230*, 111202. [[CrossRef](#)]



© 2020 by the authors. Licensee MDPI, Basel, Switzerland. This article is an open access article distributed under the terms and conditions of the Creative Commons Attribution (CC BY) license (<http://creativecommons.org/licenses/by/4.0/>).